

# Improved CUT&RUN chromatin profiling tools

Michael P Meers<sup>1</sup>, Terri D Bryson<sup>1,2</sup>, Jorja G Henikoff<sup>1</sup>, Steven Henikoff<sup>1,2\*</sup>

<sup>1</sup>Basic Sciences Division, Fred Hutchinson Cancer Research Center, Seattle, United States; <sup>2</sup>Howard Hughes Medical Institute, United States

**Abstract** Previously, we described a novel alternative to chromatin immunoprecipitation, CUT&RUN, in which unfixed permeabilized cells are incubated with antibody, followed by binding of a protein A-Micrococcal Nuclease (pA/MNase) fusion protein (Skene and Henikoff, 2017). Here we introduce three enhancements to CUT&RUN: A hybrid protein A-Protein G-MNase construct that expands antibody compatibility and simplifies purification, a modified digestion protocol that inhibits premature release of the nuclease-bound complex, and a calibration strategy based on carry-over of *E. coli* DNA introduced with the fusion protein. These new features, coupled with the previously described low-cost, high efficiency, high reproducibility and high-throughput capability of CUT&RUN make it the method of choice for routine epigenomic profiling.

DOI: <https://doi.org/10.7554/eLife.46314.001>

## Introduction

Profiling the chromatin landscape for specific components is one of the most widely used methods in biology, and over the past decade, chromatin immunoprecipitation (ChIP) followed by sequencing (ChIP-seq) has become practically synonymous with genome-wide chromatin profiling (Landt et al., 2012; Schubert, 2018). However, the most widely used ChIP-seq protocols have limitations and are subject to artifacts (Jain et al., 2015; Park et al., 2013; Teves et al., 2016; Teytelman et al., 2013), of which only some have been addressed by methodological improvements (Brind'Amour et al., 2015; Kasinathan et al., 2014; Rhee and Pugh, 2011; Rossi et al., 2018; van Galen et al., 2016). An inherent limitation to ChIP is that solubilization of chromatin, whether by sonication or enzymatic digestion, results in sampling from the entire solubilized genome, and this requires very deep sequencing so that the sites of targeted protein binding can be resolved above background (Landt et al., 2012). To overcome this limitation, we introduced Cleavage Under Targets and Release Using Nuclease (CUT&RUN) (Skene and Henikoff, 2017), which is based on the chromatin immunocleavage (ChIC)-targeted nuclease strategy (Schmid et al., 2004): Successive incubation of unfixed cells or nuclei with an antibody and a Protein A-Micrococcal Nuclease (pA/MNase) fusion protein is followed by activation of MNase with calcium. In CUT&RUN, cells or nuclei remain intact throughout the procedure and only the targeted sites of binding are released into solution. Our CUT&RUN method dramatically reduced non-specific backgrounds, such that ~10 fold lower sequencing depth was required to obtain similar peak-calling performance (Skene and Henikoff, 2017). In addition, CUT&RUN provides near base-pair resolution, and our most recently published benchtop protocol is capable of profiling ~100 human cells for an abundant histone modification and ~1000 cells for a transcription factor (Skene et al., 2018). The simplicity of CUT&RUN has also resulted in a fully automated robotic version (AutoCUT&RUN) in which the high reproducibility and low cost makes it ideally suited for high-throughput epigenomic profiling of clinical samples (Janssens et al., 2018). Other advances based on our original CUT&RUN publication include CUT&RUN.Salt for fractionation of chromatin based on solubility (Thakur and Henikoff, 2018) and CUT&RUN.ChIP for profiling specific protein components within complexes released by CUT&RUN

\*For correspondence:  
steveh@fhcrc.org

**Competing interests:** The authors declare that no competing interests exist.

**Funding:** See page 13

**Received:** 22 February 2019

**Accepted:** 22 June 2019

**Published:** 24 June 2019

**Reviewing editor:** Stephen Parker, University of Michigan, United States

© Copyright Meers et al. This article is distributed under the terms of the [Creative Commons Attribution License](https://creativecommons.org/licenses/by/4.0/), which permits unrestricted use and redistribution provided that the original author and source are credited.

digestion (*Brahma and Henikoff, 2019*). CUT&RUN has also been adopted by others (*Ahmad and Spens, 2018; Daneshvar et al., 2019; de Bock et al., 2018; Ernst et al., 2019; Federation et al., 2018; Hainer et al., 2019; Hainer and Fazio, 2019; Hyle et al., 2019; Inoue et al., 2018; Liu et al., 2018; Menon et al., 2019; Oomen et al., 2019; Park et al., 2019; Roth et al., 2018; Uyehara and McKay, 2019; Zhang et al., 2019; Zheng and Gehring, 2019*), and since publication of our eLife paper we have distributed materials to >600 laboratories world-wide, with user questions and answers fielded interactively on our open-access Protocols.io site ([dx.doi.org/10.17504/protocols.io.zcpf2vn](https://dx.doi.org/10.17504/protocols.io.zcpf2vn)).

Broad implementation of CUT&RUN requires reagent standardization, and the rapid adoption of CUT&RUN by the larger community of researchers motivates the enhancements described here. First, the method requires a fusion protein that is not at this writing commercially available, and the published pA/MNase purification protocol is cumbersome, which effectively restricts dissemination of the method. Therefore, we have produced an improved construct with a 6-His-Tag that can be easily purified using a commercial kit, and by using a Protein A-Protein G hybrid, the fusion protein binds avidly to mouse antibodies, which bind only weakly to Protein A. Second, the original protocols are sensitive to digestion time, in that under-digestion results in low yield and over-digestion can result in pre-mature release of pA/MNase-bound complexes that can digest accessible DNA sites. To address this limitation, we have modified the protocol such that premature release is reduced, allowing digestion to near-completion for high yields with less background. Third, the current CUT&RUN protocol recommends a spike-in of heterologous DNA at the release step to compare samples in a series. Here we demonstrate that adding a spike-in is unnecessary, because the carry-over of *E. coli* DNA from purification of pA/MNase or pAG/MNase is sufficient to calibrate samples in a series.

## Results and discussion

### An improved CUT&RUN vector

The pA/MNase fusion protein produced by the pK19-pA-MN plasmid (*Schmid et al., 2004*) requires purification from lysates of *Escherichia coli* overexpressing cells using an immunoglobulin G (IgG) column, and elution with low pH followed by neutralization has resulted in variations between batches. To improve the purification protocol, we added a 6-His tag (*Bornhorst and Falke, 2000*) into the pK19-pA-MN fusion protein (*Figure 1A* and *Figure 1—figure supplement 1A*). This allowed for simple and gentle purification on a nickel resin column (*Figure 1—figure supplement 1B*). In addition, we found that a commercial 6-His-cobalt resin kit also yielded pure highly active enzyme from a 20 ml culture, enough for ~10,000 reactions. Even when used in excess, there is no increase in release of background fragments (*Figure 1—figure supplement 2*), which indicates that the washes are effective in removing unbound fusion protein.

In principle an epitope-tagged pAG/MNase could be used for chromatin pull-down from a CUT&RUN supernatant in sequential strategies like CUT&RUN.ChIP (*Brahma and Henikoff, 2019*). However, in practice use of the 6-His tag is complicated by the requirement for a chelating agent to release the protein from the nickel resin. Therefore, we also added an HA (hemagglutinin) tag, which could be used to affinity-purify the complex of a directly bound chromatin particle with a primary antibody and the fusion protein.

Protein A binds well to rabbit, goat, donkey and guinea pig IgG antibodies, but poorly to mouse IgG1, and so for most mouse antibodies, Protein G is generally used (*Fishman and Berg, 2019*). To further improve the versatility of the MNase fusion protein, we encoded a single Protein G domain adjacent to the Protein A domain in the pK19-pA-MN plasmid (*Eliasson et al., 1988*). In addition, we mutated three residues in the Protein G coding sequence to further increase binding for rabbit antibodies (*Jha et al., 2014*). This resulted in a fusion protein that binds strongly to most commercial antibodies without requiring a secondary antibody. We found that for ordinary CUT&RUN applications pAG/MNase behaves very similarly to pA/MNase, but is more easily purified and is more versatile, for example allowing us to perform CUT&RUN without requiring a secondary antibody for mouse primary monoclonal antibodies (*Figure 1B*).

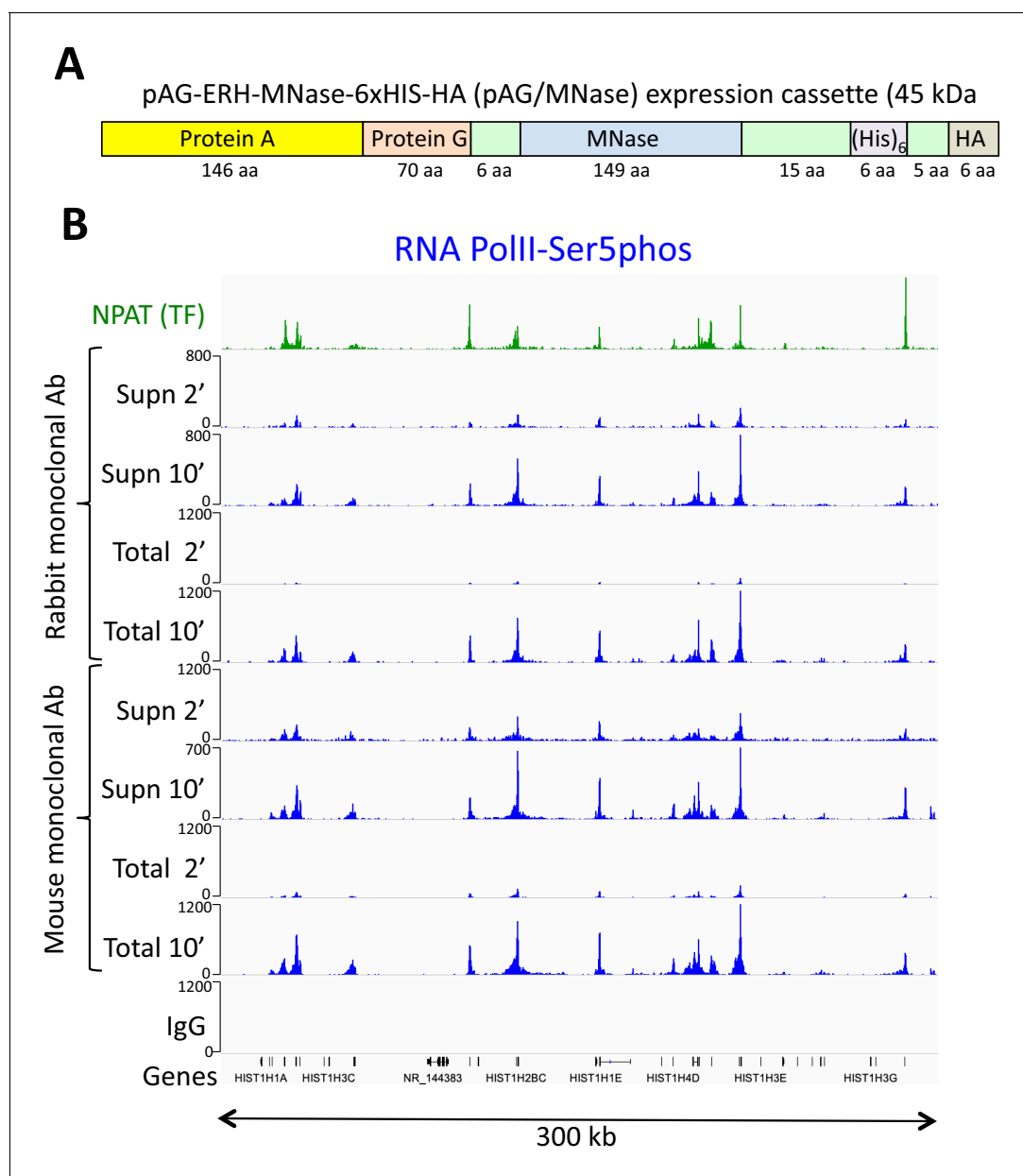


**Figure 1.** An improved fusion protein for CUT&RUN. (A) Schematic diagram (not to scale) showing improvements to the pA-MNase fusion protein, which include addition of the C2 Protein G IgG binding domain, a 6-histidine tag for purification and a hemagglutinin tag (HA) for immunoprecipitation. (B) The Protein A/G hybrid fusion results in high-efficiency CUT&RUN for both rabbit and mouse primary antibodies. CUT&RUN for both rabbit and mouse RNAPII-Ser5phosphate using pAG/MNase were extracted from either the supernatant or the total cellular extract. Tracks are shown for the histone gene cluster at Chr6:26,000,000–26,300,000, where NPAT is a transcription factor that co-activates histone genes. Tracks for 2' and 10' time points are displayed at the same scale for each antibody and for both supernatant (supn) or total DNA extraction protocols.

DOI: <https://doi.org/10.7554/eLife.46314.002>

The following figure supplements are available for figure 1:

**Figure supplement 1.** An improved fusion protein for CUT&RUN.

DOI: <https://doi.org/10.7554/eLife.46314.003>

**Figure supplement 2.** pAG/MNase titration.

DOI: <https://doi.org/10.7554/eLife.46314.004>

## Preventing premature release during CUT&RUN digestion

When fragments are released by cleavage in the presence of  $\text{Ca}^{++}$  ions, the associated pA/MNase complex can digest accessible DNA (*Skene and Henikoff, 2017*). Although performing digestion at  $0^\circ\text{C}$  minimizes this artifact, eliminating premature release during digestion would allow for more complete release of target-specific fragments. Based on the observation that nucleosome core particles aggregate in high-divalent-cation and low-salt conditions (*de Frutos et al., 2001*), we wondered whether these conditions would prevent premature release of chromatin particles in situ. Therefore, we performed digestions in 10 mM  $\text{CaCl}_2$  and 3.5 mM HEPES pH 7.5. Under these high-calcium/low-salt conditions, chromatin is digested with no detectable release of fragments into the supernatant (*Figure 2*). Reactions are halted by transferring the tube to a magnet, removing the liquid, and adding elution buffer containing 150 mM NaCl, 20 mM EGTA and 25  $\mu\text{g/ml}$  RNAse A, which releases the small DNA fragments into the supernatant. These conditions are compatible with direct end-polishing and ligation used for AutoCUT&RUN (*Janssens et al., 2018*). Furthermore, retention of the cleaved fragments within the nucleus under high-divalent cation/low-salt conditions could facilitate single-cell application of CUT&RUN.

The high-calcium/low-salt protocol provided similar results using either pA/MNase and pAG/MNase (*Figure 3*). We also obtained similar results with either protocol for digestion time points over a  $\sim 30$  fold range and for both supernatant and total DNA extraction (*Figure 4—figure supplement 1*). For antibodies to H3K27ac, libraries produced using the high-calcium/low-salt protocol showed improved consistency relative to the standard protocol when digested over an extended time-course (*Figure 4*), presumably because preventing release of particles during digestion avoids their premature release where they would artifactually digest accessible DNA. The close correlations between high-calcium/low-salt H3K27ac datasets for time points over a  $\sim 100$  fold range occur with corresponding increases in the yield of fragments released into the supernatant during subsequent elution (*Figure 4—figure supplement 2*). This indicates that longer digestion times result in higher yields, with high signal-to-noise throughout the digestion series (*Figure 4*). Thus, this modification of CUT&RUN can reduce the risk of overdigestion for abundant epitopes such as H3K27ac, where premature release of pA-MNase-bound chromatin particles can increase background.

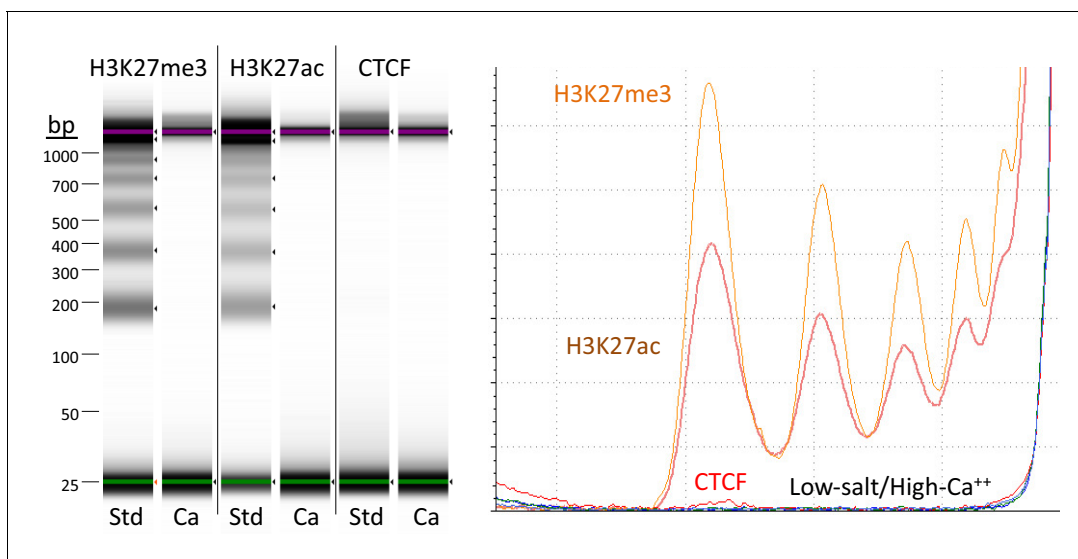


**Figure 2.** Targeted fragments are not released during digestion using high-calcium/low-salt conditions. CUT&RUN was performed using either the high- $\text{Ca}^{++}$ /low-salt ( $\text{Ca}^{++}$ ) or the standard (Std) method with antibodies to three different epitopes. DNA was extracted from supernatants, where no elution was carried out for the  $\text{Ca}^{++}$  samples. Although high yields of nucleosomal ladder DNA eluted from the supernatants using the standard method, no DNA was detectable in the supernatant using the high- $\text{Ca}^{++}$ /low salt method when the elution step was omitted. Left, Tapestation images from indicated lanes; Right, Densitometry of the same lanes.

DOI: <https://doi.org/10.7554/eLife.46314.005>

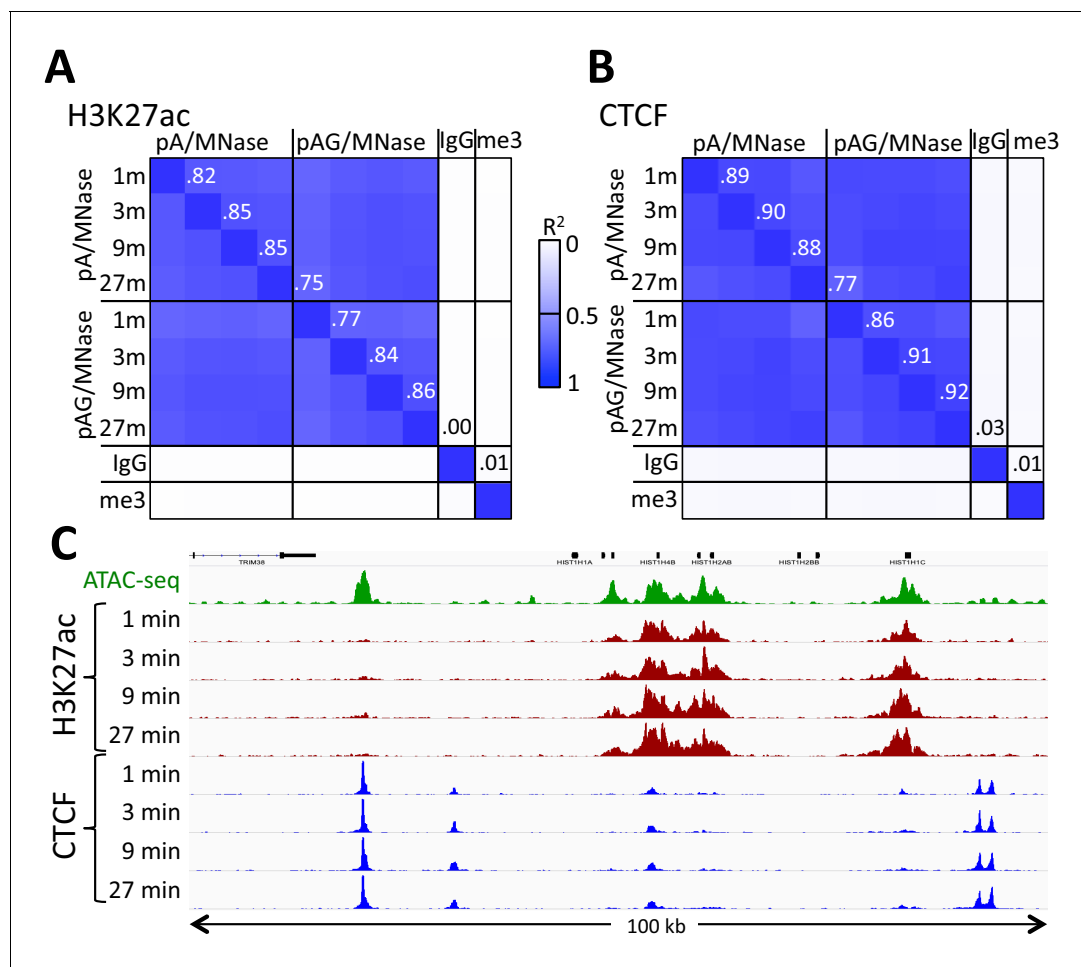


**Figure 3.** Similar performance using pA/MNase and pAG/MNase. (A) CUT&RUN was performed with an antibody to H3K27ac (Millipore MABE647) and to CTCF (Millipore 07-729) with digestion over a 1 to 27 min range as indicated using pAG/MNase with the high- $\text{Ca}^{++}$ /low-salt protocol. Correlation matrix comparing peak overlaps for time points and fusion constructs. The datasets were pooled and MACS2 was used with default parameters to call peaks, excluding those in repeat-masked intervals and those where peaks overlapped with the top 1% of IgG occupancies, for a total of 52,425 peaks. Peak positions were scored for each dataset and correlations ( $R^2$  values shown along the diagonal and displayed with Java TreeView v.1.16r2, contrast = 1.25) were calculated between peak vectors. IgG and H3K27me3 (me3) negative controls were similarly scored. (B) Same as A, except the antibody was to CTCF. A set of 9403 sites with a CTCF motif within a hypersensitive site was used (Skene and Henikoff, 2017). High correlations between all time points demonstrate the uniformity of digestion over a 27-fold range. (C) Representative tracks from datasets used for panels A and B showing a 100 kb region that includes a histone locus cluster (chr6:25,972,600–26,072,600).

DOI: <https://doi.org/10.7554/eLife.46314.006>

We previously showed that CUT&RUN can be performed on insoluble protein complexes by extracting total DNA (Skene and Henikoff, 2017) or by performing salt fractionation of the bead-bound cells and extracting DNA from the residual pellet (Thakur and Henikoff, 2018). In either case, large DNA fragments were depleted using SPRI (AMPure XP) beads before library preparation. RNA polymerase II (RNAPII) from animal cells is insoluble when engaged (Mayer et al., 2015; Weber et al., 2014), and requires harsh treatments for quantitative profiling using ChIP (Skene and Henikoff, 2015). To determine whether CUT&RUN can be used for insoluble chromatin complexes, we profiled Serine-5-phosphate on the C-terminal domain (CTD) of the Rpb1 subunit of RNAPII using both extraction of supernatant and of total DNA. This CTD phosphorylation is enriched in the initiating form of RNAPII, and we observed similar genic profiles for supernatant and total DNA (Figure 1B).

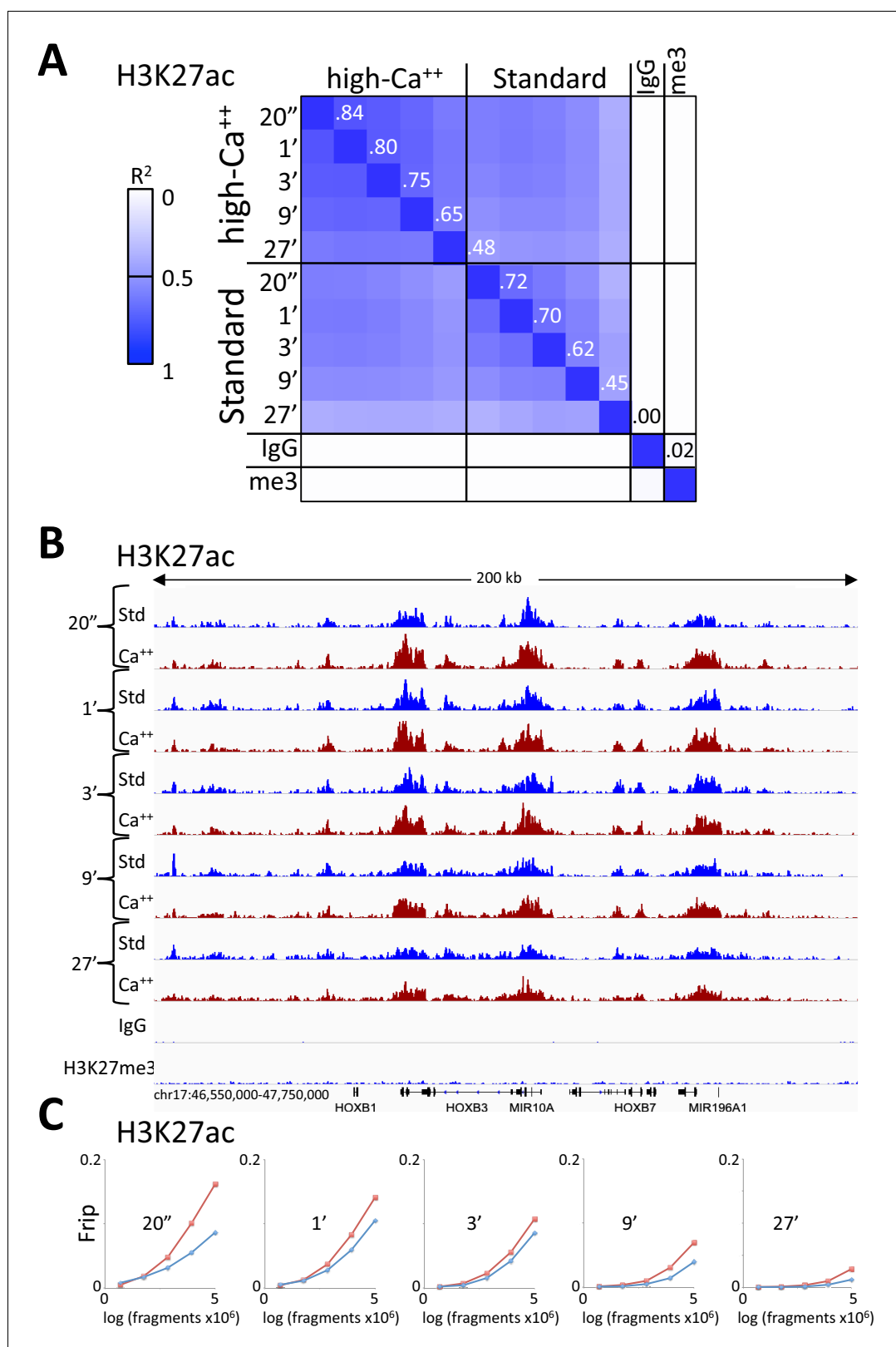


**Figure 4.** Consistent peak definition with high-Ca<sup>++</sup>/low salt digestion. (A) H3K27ac CUT&RUN time-course experiments were performed with an Abcam 4729 rabbit polyclonal antibody, following either the standard protocol or the low-salt/high-calcium (High-Ca<sup>++</sup>) protocol. Samples of 5 million fragments from the 10 H3K27ac datasets were pooled and MACS2 called 36,529 peaks. Peak positions were scored for each dataset and Figure 4 continued on next page

Figure 4 continued

correlations ( $R^2$  values shown along the diagonal) were calculated between peak vectors. IgG and H3K27me3 (me3) negative controls were similarly scored. Higher correlations between the High-Ca<sup>++</sup> than the Standard time points indicates improved uniformity of digestion over the ~100 fold range of digestion times. (B) Tracks from a representative 200 kb region around the HoxB locus. (C) Fraction of reads in peaks (Frip) plots for each time point after down-sampling (5 million, 2.5 million, 1.25 million, 625,000 and 312,500), showing consistently higher Frip values for Ca<sup>++</sup> (red) than Std (blue).

DOI: <https://doi.org/10.7554/eLife.46314.007>

The following figure supplements are available for figure 4:

**Figure supplement 1.** CUT&RUN consistency with high-Ca<sup>++</sup>/low salt digestion and total DNA extraction.

DOI: <https://doi.org/10.7554/eLife.46314.008>

**Figure supplement 2.** Tapestation analyses of an H3K27ac digestion time-course series.

DOI: <https://doi.org/10.7554/eLife.46314.009>

## Calibration using *E. coli* carry-over DNA

Comparing samples in a series typically requires calibration for experimental quality and sequencing read depth. It is common to use background levels to calibrate ChIP-seq samples in a series and to define and compare peaks for peak-calling (Landt et al., 2012). However, the extremely low backgrounds of CUT&RUN led us to a calibration strategy based on spike-in of heterologous DNA, which has been generally recommended for all situations in which samples in a series are to be compared (Chen et al., 2015; Hu et al., 2015). In our current spike-in protocol, the heterologous DNA, which is typically DNA purified from an MNase digest of yeast *Saccharomyces cerevisiae* or *Drosophila melanogaster* chromatin, is added when stopping a reaction, and we adopted this spike-in procedure for the high-calcium/low-salt protocol described in the previous section. Interestingly, we noticed that mapping reads to both the spike-in genome and the *E. coli* genome resulted in almost perfect correlation ( $R^2 = 0.97$ ) between *S. cerevisiae* and *E. coli* in an experiment using pA/MNase in which the number of cells was varied over several orders of magnitude (Figure 5A). Near-perfect correlations ( $R^2 = 0.96$ – $0.99$ ) between yeast spike-in and carry-over *E. coli* DNA were also seen in series using the same batch of pAG/MNase with high-calcium/low-salt digestion conditions (Figure 5B), and for both supernatant release and extraction and total DNA extraction (Figure 5C–D). These strong positive correlations are not accounted for by cross-mapping of the yeast spike-in to the *E. coli* genome, because omitting the spike-in for a low-abundance epitope resulted in very few yeast counts with high levels of *E. coli* counts (blue symbol in Figure 5C–D panels). As the source of *E. coli* DNA is carried over from purification of pA/MNase and pAG/MNase, the close correspondence provides confirmation of the accuracy of our heterologous spike-in procedure (Skene and Henikoff, 2017). Moreover, as carry-over *E. coli* DNA is introduced at an earlier step, and is cleaved to small mappable fragments that are released during digestion and elution, it provides a more desirable calibration standard than using heterologous DNA (Chen et al., 2015; Hu et al., 2015). High correlations were also seen between *S. cerevisiae* spike-in and *E. coli* carry-over DNA for pA-MNase in batches that we have distributed (Table 1). Therefore, data for nearly all CUT&RUN experiments performed thus far can be recalibrated *post-hoc* whether or not a spike-in calibration standard had been added.

To explain the presence of carry-over *E. coli* DNA in proportion to the amount of yeast spike-in DNA, which is constant between samples in a series, we can exclude intracellular binding, because we observe proportionality between *E. coli* and yeast reads despite varying human cell numbers over two orders of magnitude (Figure 5A). Rather, we note that Concanavalin A binds to glycosylated immunoglobulins, and so the successive treatments of Con A bead-bound cells with excess antibody and Protein A(G)/MNase fusion protein will affix an amount of carry-over *E. coli* DNA to beads in proportion to the number of beads. Our use of a constant number of beads for all samples in a series to be compared would then have resulted in a constant amount of carry-over *E. coli* DNA. A similar inference of *E. coli* carry-over DNA suitable for calibration was noted for CUT&Tag (Kaya-Okur et al., 2019), which suggests successive binding of antibodies and Protein A-Tn5 to the Con A beads used to immobilize cells. Thus, our calibration strategy might serve as a more general replacement for conventional spike-ins.

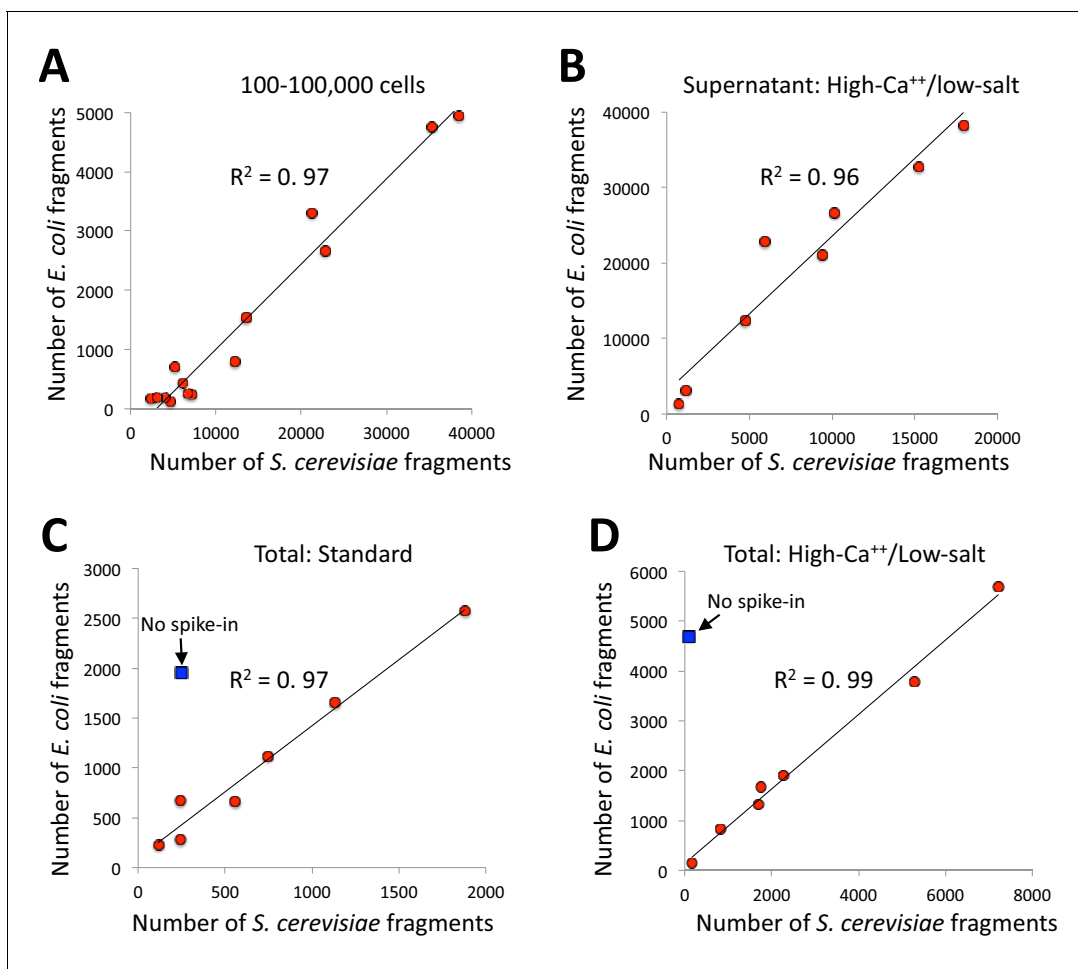


**Figure 5.** *E. coli* carry-over DNA of pA/MNase and pAG/MNase can substitute for spike-in calibration. (A) Fragments from a CUT&RUN K562 cell experiment (GSE104550 20170426) using antibodies against H3K27me3 (100–8,000 cells) and CTCF (1,000–100,000 cells) were mapped to the repeat-masked genome of *S. cerevisiae* and the full genome of *E. coli*. Standard digestion was followed by supernatant release and extraction. (B) Same as A using antibodies against multiple epitopes of varying abundances, with high-calcium/low-salt digestion followed by supernatant release and extraction. (C) Same as B except using standard digestion conditions and total DNA extraction. The *S. cerevisiae* spike-in DNA was left out for one sample (blue square). From top to bottom, antibodies are: NPAT Thermo PA5-66839, Myc: CST Rabbit Mab #13987, CTD: PolII CTD Abcam 8WG16, RNAPII-Ser5: Abcam 5408 (mouse), RNAPII-Ser2: CST E1Z3G, CTCF Millipore 07–729, RNAPII-Ser5: CST D9N5I (rabbit), H3K4me2: Upstate 07–030. (D) Same as C except using high-calcium/low-salt digestion and total DNA extraction. From top to bottom, antibodies are: CTCF Millipore 07–729, NPAT Thermo PA5-66839, Myc: CST Rabbit Mab #13987, CTD: PolII CTD Abcam 8WG16, RNAPII-Ser5: Abcam 5408 (mouse), RNAPII-Ser5: CST D9N5I (rabbit), RNAPII-Ser2: CST E1Z3G, H3K4me2: Upstate 07–030.

DOI: <https://doi.org/10.7554/eLife.46314.010>

## Conclusions

Since its introduction in our original *eLife* paper (Skene and Henikoff, 2017), the advantages of CUT&RUN over ChIP-seq has led to its rapid adoption, including publication of new CUT&RUN protocols for low cell numbers (Hainer and Fazio, 2019; Skene et al., 2018), for plant tissues (Zheng and Gehring, 2019) and for high-throughput (Janssens et al., 2018). The new CUT&RUN advances that we describe here are likely to be useful when applied in all of these protocols. Our improved CUT&RUN fusion construct simplifies reagent purification and eliminates the requirement for a secondary antibody against mouse primary antibodies. Our high-calcium/low-salt protocol minimizes time-dependent variability. Our discovery that carry-over *E. coli* DNA almost perfectly correlates with an added spike-in upgrades a contaminant to a resource that can be used as a spike-in calibration proxy, even *post-hoc* simply by counting reads mapping to the *E. coli* genome in existing CUT&RUN datasets.

**Table 1.** Carry-over *E. coli* DNA correlates closely with the heterologous spike-in for both fusion proteins and both low-salt/high-calcium and standard digestion conditions.

CUT&RUN was performed for H3K27me3 in parallel for pA/MNase Batch #6 (pA), pAG/MNase (pAG) using both low-salt/high-calcium (lo-hi) and standard (std) CUT&RUN digestion conditions. Each sample started with ~700,000 cells and 10  $\mu$ L of bead slurry. Also varied in this experiment was addition of antibody followed by bead addition (Ab first) and addition of 0.1% BSA in the antibody buffer (BSA). Adding antibody first led to increased recovery of both yeast and *E. coli* DNA relative to human DNA, indicative of loss of cells prior to addition of fusion protein, possibly caused by loss of digitonin solubilization of membrane sugars.

H3K27me3	Ab first	BSA	Human	Yeast	<i>E. coli</i>	Corr (Sc:Ec)
pA lo-hi			5913983	743	3455	0.92
pA lo-hi		+	7748003	858	4988	
pA lo-hi	+		5202278	2288	16110	
pA lo-hi	+	+	5178086	1804	18759	
pA std			6013347	595	2462	0.99
pA std		+	6005080	859	2295	
pA std	+		4104736	2624	21236	
pA std	+	+	3972820	2328	19245	
pAG lo-hi			6999802	789	404	0.94
pAG lo-hi		+	6374939	642	467	
pAG lo-hi	+		4140407	1565	1291	
pAG lo-hi	+	+	4058693	2382	5289	
pAG std			7514127	308	567	0.90
pAG std		+	5935592	355	125	
pAG std	+		4594153	1271	555	
pAG std	+	+	5379610	2509	1353	

DOI: <https://doi.org/10.7554/eLife.46314.011>

## Materials and methods

### Key resources table

Reagent type (species) or resource	Designation	Source or reference	Identifiers	Additional information
Cell line (Human)	K562	ATCC	#CCL-243	RRID: <a href="#">CVCL_0004</a>
Biological sample ( <i>Escherichia coli</i> )	JM101 cells	Agilent	#200234	
Antibody	rabbit polyclonal anti-NPAT	Thermo	PA5-66839	Concentration: 1:100; RRID: <a href="#">AB_2663287</a>
Antibody	guinea pig polyclonal anti-rabbit IgG	Antibodies Online	ABIN101961	Concentration: 1:100; RRID: <a href="#">AB_10775589</a>
Antibody	rabbit polyclonal anti-mouse IgG	Abcam	46540	Concentration: 1:100; RRID: <a href="#">AB_2614925</a>
Antibody	rabbit monoclonal anti-RNAPII-Ser5	Cell Signaling	D9N51	Concentration: 1:100
Antibody	mouse monoclonal anti-RNAPII-Ser5	Abcam	5408	Concentration: 1:100; RRID: <a href="#">AB_304868</a>
Antibody	rabbit monoclonal anti-H3K27me3	Cell Signaling	9733	Concentration: 1:100; RRID: <a href="#">AB_2616029</a>
Antibody	rabbit polyclonal anti-H3K4me2	Upstate	07-730	Concentration: 1:100; RRID: <a href="#">AB_11213050</a>

Continued on next page

Continued

Reagent type (species) or resource	Designation	Source or reference	Identifiers	Additional information
Antibody	rabbit monoclonal anti-H3K27ac	Millipore	MABE647	Concentration: 1:100;
Antibody	rabbit polyclonal anti-H3K27ac	Abcam	4729	Concentration: 1:100; RRID: <a href="#">AB_2118291</a>
Antibody	rabbit polyclonal anti-CTCF	Millipore	07-729	Concentration: 1:100; RRID: <a href="#">AB_441965</a>
Recombinant DNA reagent	AG-ERH-MNase-6xHIS-HA (plasmid)		Progenitors: pK19-pA-MN; gBlocks	
Recombinant DNA reagent	pK19-pA-MN	<i>Schmid et al., 2004</i>		Gift from author
Sequence-based reagent	gBlock Hemagglutinin and 6-histidine tags; gattaca GAAGACAACGCTGATTTCAG GTCAAGGCGGtGGTGGcTC TGGgGGcGGgGGcTCGGGtG GtGGgGGcTCAccatcacatca ccatGGCGGtGGTGGcTCTT ACCCATACGATGTTCCAGA TTACGCTtaatgaGGATCCgattaca	Integrated DNA Technologies (IDT)		
Sequence-based reagent	gBLOCK PrtG_ERH Codon optimized; AGCAGAAGCTAAAAAGCTAAACGA TGCTCAAGCACCAAAAACAATTAT AAATTAGTCATCAACGGGAAAACGC TGAAGGGTGA AACCCACGACAGAGG CCGTAGATGCGGAGACAGCGGAGC GCCACTTTAAGCAATACGCGAATG ATAACGGTGTAGACGGCGAGTGGC CCTACGACGACGCGACAAAGACCT TTACCGTCACGGAGAACCTGAGG TTATCGACGCGTCTGAGTTGACGC CAGCCGTAGATGACGATAAAGAAT TCGCAACTTCAACTAAAAAATTAC	Integrated DNA Technologies (IDT)		
Peptide, recombinant protein	pA/MNase	<i>Schmid et al., 2004</i>		purified as described in <i>Schmid et al., 2004</i> and supplementary
Peptide, recombinant protein	pAG/MNase	This paper		Purified from modified plasmid pAG-ERH-MNase-6xHIS-HA in S Henikoff Lab
Commercial assay or kit	Pull-Down PolyHis Protein:Protein Interaction Kit	Thermo	#21277	
Other	Concanavalin A coated magnetic beads	Bangs Laboratories	#BP-531	
Other	Gibson Assembly	New England Biolabs	#E2611	
Other	Chicken egg white lysozyme	EMD Millipore	#71412	
Other	Zwittergent 3-10 detergent (0.03%)	EMD Millipore	#693021	
Chemical compound, drug	Digitonin	EMD Millipore	#300410	
Chemical compound, drug	Roche Complete Protease Inhibitor EDTA-free tablets	Sigma Aldrich	5056489001	

Continued on next page

Continued

Reagent type (species) or resource	Designation	Source or reference	Identifiers	Additional information
Chemical compound, drug	RNase A Dnase- and protease-free	Thermo	ENO531	10 mg/ml
Chemical compound, drug	Proteinase K	Thermo	EO0492	
Chemical compound, drug	Glycogen	Sigma-Aldrich	10930193001	
Chemical compound, drug	Spermidine	Sigma-Aldrich	#S0266	

## Cell culture

K562 cells were purchased from ATCC (#CCL-243) and cultured as previously described (Janssens *et al.*, 2018). All tested negative for mycoplasma contamination using MycoProbe kit.

## Construction and purification of an improved IgG-affinity/MNase fusion protein

Hemagglutinin and 6-histidine tags were added to the carboxyl-terminus of pA-MNase (Schmid *et al.*, 2004) using a commercially synthesized dsDNA fragment (gBlock) from Integrated DNA Technologies (IDT), which contains the coding sequence for both tags, glycine-rich flexible linkers and includes restriction sites for cloning. Another IDT gBlock containing the optimized protein-G coding sequence and homologous flanking regions to the site of insertion, was introduced via PCR overlap extension using Gibson Assembly Master Mix (New England Biolabs cat. #E2611), following the manufacturer's instructions. The sequence-verified construct was transformed into JM101 cells (Agilent Technologies cat. #200234) for expression, cultured in NZCYM-Kanamycin (50 µg/ml) and induced with 2 mM Isopropyl β-D-1-thiogalactopyranoside following standard protein expression and purification protocols. The cell pellet was resuspended in 10 ml Lysis Buffer, consisting of 10 mM Tris-HCl pH 7.5, 300 mM NaCl, 10 mM Imidazole, 5 mM beta-mercaptoethanol, and EDTA-free protease inhibitor tablets at the recommended concentration (Sigma-Aldrich cat. #5056489001). Lysis using chicken egg white lysozyme (10 mg/mL solution, EMD cat. #71412 solution) was followed by sonication with a Branson Sonifier blunt-end adapter at output level 4, 45 s intervals for 5–10 rounds or until turbidity was reduced. The lysate was cleared by high-speed centrifugation and purified over a nickel-agarose column, taking advantage of the poly-histidine tag for efficient purification via immobilized metal affinity chromatography. Cleared lysate was applied to a 20 ml disposable gravity-flow column 1.5 ml (0.75 ml bed volume) of NI-NTA agarose (Qiagen cat. #30210), washed twice in three bed volumes of Lysis Buffer. Lysate was applied followed by two washes at five bed volumes of 10 mM Tris-HCl pH 7.5, 300 mM NaCl, 20 mM Imidazole, 0.03% ZWITTERGENT 3–10 Detergent (EMD Millipore cat. #693021) and EDTA-free protease inhibitor tablets. Elution was performed with 1 ml 10 mM Tris-HCl pH 7.5, 300 mM NaCl, 250 mM Imidazole and EDTA-free protease inhibitor tablets. Eluate was dialyzed twice against a 750 ml volume of 10 mM Tris-HCl pH 7.5, 150 mM NaCl, 1 mM EDTA, 1 mM PMSF to remove imidazole. Glycerol was then added to 50%, aliquots stored at –80°C for long term storage and –20°C for working stocks.

For purification, we used either the nickel-based protocol or the Pierce Cobalt kit (Pull-Down PolyHis Protein:Protein Interaction Kit cat. #21277 from Thermo Fisher). Similar results were obtained using either the nickel or cobalt protocol, although the cobalt kit alleviated the need for a sonicator, using a fifth of the starting material from either fresh culture or a cell pellet frozen in lysis buffer, and yielded more protein per volume of starting material. With the cobalt kit, 20 ml of culture yielded ~100 µg of fusion protein.

## CUT&RUN using high-calcium/low-salt digestion conditions

Log-phase cultures of K562 cells were harvested, washed, and bound to activated Concanavalin A-coated magnetic beads, then permeabilized with Wash buffer (20 mM HEPES, pH7.5, 150 mM NaCl, 0.5 mM spermidine and a Roche complete tablet per 50 ml) containing 0.05% Digitonin (Dig-Wash) as described (Skene *et al.*, 2018). The bead-cell slurry was incubated with antibody in a 50–



7. Removed peaks from macs2 results in step four if the mean score was greater than the 99th percentile of all IgG scores to make a subset of the peaks lacking the most extreme outliers.
8. Extracted bedgraph values for  $\pm 150$  bps around the subset of peak summits from step seven for all samples and computed their means, which resulted in a matrix with columns corresponding to samples and one row per peak.
9. Computed correlations of matrix in eight using R 3.2.2 `cor(matrix, use='complete.obs')` command.

## Acknowledgements

We thank Christine Codomo and Tayler Hentges for technical support. We also thank all members of the Henikoff lab for valuable discussions and Kami Ahmad, Brian Freie and Bob Eisenman for comments on the manuscript. This work was supported by the Howard Hughes Medical Institute, and a grant from the National Institutes of Health (4DN TCPA A093) and the Chan-Zuckerberg Initiative.

---

## Additional information

### Funding

Funder	Grant reference number	Author
Howard Hughes Medical Institute		Steven Henikoff
National Institutes of Health	4DN TCPA A093	Steven Henikoff
Chan-Zuckerberg Initiative		Steven Henikoff

The funders had no role in study design, data collection and interpretation, or the decision to submit the work for publication.

### Author contributions

Michael P Meers, Validation, Writing—review and editing; Terri D Bryson, Investigation, Methodology, Writing—original draft, Writing—review and editing; Jorja G Henikoff, Data curation, Software, Formal analysis, Writing—review and editing; Steven Henikoff, Conceptualization, Resources, Supervision, Funding acquisition, Validation, Investigation, Visualization, Methodology, Writing—original draft, Writing—review and editing

### Author ORCIDs

Steven Henikoff  <https://orcid.org/0000-0002-7621-8685>

### Decision letter and Author response

Decision letter <https://doi.org/10.7554/eLife.46314.017>

Author response <https://doi.org/10.7554/eLife.46314.018>

---

## Additional files

### Supplementary files

- Transparent reporting form

DOI: <https://doi.org/10.7554/eLife.46314.012>

### Data availability

The plasmid pAG-ERH-MNase-6xHIS-HA is available from Addgene. Sequencing datasets are available from GEO (GSE126612).

The following dataset was generated:

Author(s)	Year	Dataset title	Dataset URL	Database and Identifier
Meers MP, Bryson TD, Henikoff S	2019	A streamlined protocol and analysis pipeline for CUT&RUN chromatin profiling	<a href="http://www.ncbi.nlm.nih.gov/geo/query/acc.cgi?acc=GSE126612">http://www.ncbi.nlm.nih.gov/geo/query/acc.cgi?acc=GSE126612</a>	NCBI Gene Expression Omnibus, GSE126612

## References

- Ahmad K, Spens A. 2018. Separate polycomb response elements control chromatin state and activation of the vestigial gene. *bioRxiv*. DOI: <https://doi.org/10.1101/488478>
- Bornhorst JA, Falke JJ. 2000. Purification of proteins using polyhistidine affinity tags. *Methods in Enzymology* **326**:245–254. DOI: <https://doi.org/10.1016/j.pep.2011.08.022>, PMID: 11036646
- Brahma S, Henikoff S. 2019. RSC-Associated subnucleosomes define MNase-Sensitive promoters in yeast. *Molecular Cell* **73**:238–249. DOI: <https://doi.org/10.1016/j.molcel.2018.10.046>, PMID: 30554944
- Brind'Amour J, Liu S, Hudson M, Chen C, Karimi MM, Lorincz MC. 2015. An ultra-low-input native ChIP-seq protocol for genome-wide profiling of rare cell populations. *Nature Communications* **6**:6033. DOI: <https://doi.org/10.1038/ncomms7033>, PMID: 25607992
- Chen K, Hu Z, Xia Z, Zhao D, Li W, Tyler JK. 2015. The overlooked fact: fundamental need for Spike-In control for virtually all Genome-Wide analyses. *Molecular and Cellular Biology* **36**:662–667. DOI: <https://doi.org/10.1128/MCB.00970-14>, PMID: 26711261
- Daneshvar K, Ardehal MV, Klein IA, Kratkiewicz AJ, Zhou C, Mahpour A, Cook BM, Li W, Pondick JV, Moran SP. 2019. lncRNA DIGIT and BRD3 protein form phase-separated condensates to regulate endoderm differentiation. *bioRxiv*. DOI: <https://doi.org/10.1101/547513>
- de Bock CE, Demeyer S, Degryse S, Verbeke D, Sweron B, Gielen O, Vandepoel R, Vicente C, Vanden Bempt M, Dagklis A, Geerdens E, Bornschein S, Gijssbers R, Soulier J, Meijerink JP, Heinäniemi M, Teppo S, Bouvy-Liivrand M, Lohi O, Radaelli E, et al. 2018. HOXA9 cooperates with activated JAK/STAT signaling to drive leukemia development. *Cancer Discovery* **8**:616–631. DOI: <https://doi.org/10.1158/2159-8290.CD-17-0583>, PMID: 29496663
- de Frutos M, Raspaud E, Leforestier A, Livolant F. 2001. Aggregation of nucleosomes by divalent cations. *Biophysical Journal* **81**:1127–1132. DOI: [https://doi.org/10.1016/S0006-3495\(01\)75769-4](https://doi.org/10.1016/S0006-3495(01)75769-4), PMID: 11463653
- Eliasson M, Olsson A, Palmcrantz E, Wiberg K, Inganäs M, Guss B, Lindberg M, Uhlén M. 1988. Chimeric IgG-binding receptors engineered from staphylococcal protein A and streptococcal protein G. *The Journal of Biological Chemistry* **263**:4323–4327. PMID: 2964447
- Ernst C, Eling N, Martinez-Jimenez CP, Marioni JC, Odom DT. 2019. Staged developmental mapping and X chromosome transcriptional dynamics during mouse spermatogenesis. *Nature Communications* **10**:1251. DOI: <https://doi.org/10.1038/s41467-019-09182-1>, PMID: 30890697
- Federation AJ, Nandakumar V, Wang H, Searle B, Pino L, Merrihew G, Ting S, Howard N, Kutayin T, MacCoss MJ. 2018. Quantification of nuclear protein dynamics reveals chromatin remodeling during acute protein degradation. *bioRxiv*. DOI: <https://doi.org/10.1101/345686>
- Fishman JB, Berg EA. 2019. Protein A and protein G purification of antibodies. *Cold Spring Harbor Protocols* **2019**:pdb.prot099143. DOI: <https://doi.org/10.1101/pdb.prot099143>, PMID: 30602558
- Hainer SJ, Bošković A, McCannell KN, Rando OJ, Fazio TG. 2019. Profiling of pluripotency factors in single cells and early embryos. *Cell* **177**:1319–1329. DOI: <https://doi.org/10.1016/j.cell.2019.03.014>, PMID: 30955888
- Hainer SJ, Fazio TG. 2019. High-Resolution chromatin profiling using CUT&RUN. *Current Protocols in Molecular Biology* **126**:e85. DOI: <https://doi.org/10.1002/cpmb.85>, PMID: 30688406
- Hu B, Petela N, Kurze A, Chan K-L, Chopard C, Nasmyth K. 2015. Biological chromodynamics: a general method for measuring protein occupancy across the genome by calibrating ChIP-seq. *Nucleic Acids Research* **21**:gkv670. DOI: <https://doi.org/10.1093/nar/gkv670>
- Jain J, Zhang Y, Wright S, Xu B, Shao Y, Easton J, Tian L, Feng R, Xu P, Li C. 2019. Acute depletion of CTCF directly affects MYC regulation through loss of enhancer-promoter looping. *Nucleic Acids Research*:gkz462. DOI: <https://doi.org/10.1093/nar/gkz462>, PMID: 31127282
- Inoue A, Chen Z, Yin Q, Zhang Y. 2018. Maternal eed knockout causes loss of H3K27me3 imprinting and random X inactivation in the extraembryonic cells. *Genes & Development* **32**:1525–1536. DOI: <https://doi.org/10.1101/gad.318675.118>, PMID: 30463900
- Jain D, Baldi S, Zabel A, Straub T, Becker PB. 2015. Active promoters give rise to false positive 'Phantom Peaks' in ChIP-seq experiments. *Nucleic Acids Research* **43**:6959–6968. DOI: <https://doi.org/10.1093/nar/gkv637>, PMID: 26117547
- Janssens DH, Wu SJ, Sarthy JF, Meers MP, Myers CH, Olson JM, Ahmad K, Henikoff S. 2018. Automated in situ chromatin profiling efficiently resolves cell types and gene regulatory programs. *Epigenetics & Chromatin* **11**:74. DOI: <https://doi.org/10.1186/s13072-018-0243-8>, PMID: 30577869
- Jha RK, Gaiotto T, Bradbury ARM, Strauss CEM. 2014. An improved protein G with higher affinity for human/rabbit IgG fc domains exploiting a computationally designed polar network. *Protein Engineering Design and Selection* **27**:127–134. DOI: <https://doi.org/10.1093/protein/gzu005>

- Kasinathan S**, Orsi GA, Zentner GE, Ahmad K, Henikoff S. 2014. High-resolution mapping of transcription factor binding sites on native chromatin. *Nature Methods* **11**:203–209. DOI: <https://doi.org/10.1038/nmeth.2766>, PMID: 24336359
- Kaya-Okur HS**, Wu SJ, Codomo CA, Pledger ES, Bryson TD, Henikoff JG, Ahmad K, Henikoff S. 2019. CUT&tag for efficient epigenomic profiling of small samples and single cells. *Nature Communications* **10**:1930. DOI: <https://doi.org/10.1038/s41467-019-09982-5>, PMID: 31036827
- Landt SG**, Marinov GK, Kundaje A, Kheradpour P, Pauli F, Batzoglou S, Bernstein BE, Bickel P, Brown JB, Cayting P, Chen Y, DeSalvo G, Epstein C, Fisher-Aylor KI, Euskirchen G, Gerstein M, Gertz J, Hartemink AJ, Hoffman MM, Iyer VR, et al. 2012. ChIP-seq guidelines and practices of the ENCODE and modENCODE consortia. *Genome Research* **22**:1813–1831. DOI: <https://doi.org/10.1101/gr.136184.111>, PMID: 22955991
- Liu N**, Hargreaves VV, Zhu Q, Kurland JV, Hong J, Kim W, Sher F, Macias-Trevino C, Rogers JM, Kurita R, Nakamura Y, Yuan GC, Bauer DE, Xu J, Bulyk ML, Orkin SH. 2018. Direct promoter repression by BCL11A controls the fetal to adult hemoglobin switch. *Cell* **173**:430–442. DOI: <https://doi.org/10.1016/j.cell.2018.03.016>, PMID: 29606353
- Mayer A**, di Iulio J, Maleri S, Eser U, Vierstra J, Reynolds A, Sandstrom R, Stamatoyannopoulos JA, Churchman LS. 2015. Native elongating transcript sequencing reveals human transcriptional activity at nucleotide resolution. *Cell* **161**:541–554. DOI: <https://doi.org/10.1016/j.cell.2015.03.010>, PMID: 25910208
- Menon DU**, Shibata Y, Mu W, Magnuson T. 2019. Mammalian SWI/SNF collaborates with a polycomb-associated protein to regulate male germ line transcription in the mouse. *Development*:dev.174094. DOI: <https://doi.org/10.1242/dev.174094>, PMID: 31043422
- Oomen ME**, Hansen AS, Liu Y, Darzacq X, Dekker J. 2019. CTCF sites display cell cycle-dependent dynamics in factor binding and nucleosome positioning. *Genome Research* **29**:236–249. DOI: <https://doi.org/10.1101/gr.241547.118>, PMID: 30655336
- Park D**, Lee Y, Bhupindersingh G, Iyer VR. 2013. Widespread misinterpretable ChIP-seq bias in yeast. *PLOS ONE* **8**:e83506. DOI: <https://doi.org/10.1371/journal.pone.0083506>, PMID: 24349523
- Park SM**, Cho H, Thornton AM, Barlowe TS, Chou T, Chhangawala S, Fairchild L, Taggart J, Chow A, Schurer A, Gruet A, Witkin MD, Kim JH, Shevach EM, Krivtsov A, Armstrong SA, Leslie C, Kharas MG. 2019. IKZF2 drives leukemia stem cell Self-Renewal and inhibits myeloid differentiation. *Cell Stem Cell* **24**:153–165. DOI: <https://doi.org/10.1016/j.stem.2018.10.016>, PMID: 30472158
- Rhee HS**, Pugh BF. 2011. Comprehensive genome-wide protein-DNA interactions detected at single-nucleotide resolution. *Cell* **147**:1408–1419. DOI: <https://doi.org/10.1016/j.cell.2011.11.013>, PMID: 22153082
- Rossi MJ**, Lai WKM, Pugh BF. 2018. Simplified ChIP-exo assays. *Nature Communications* **9**:2842. DOI: <https://doi.org/10.1038/s41467-018-05265-7>, PMID: 30030442
- Roth TL**, Puig-Saus C, Yu R, Shifrut E, Carnevale J, Li PJ, Hiatt J, Saco J, Krystofinski P, Li H, Tobin V, Nguyen DN, Lee MR, Putnam AL, Ferris AL, Chen JW, Schickel JN, Pellerin L, Carmody D, Alkorta-Aranburu G, et al. 2018. Reprogramming human T cell function and specificity with non-viral genome targeting. *Nature* **559**:405–409. DOI: <https://doi.org/10.1038/s41586-018-0326-5>, PMID: 29995861
- Schmid M**, Durussel T, Laemmli UK. 2004. ChIC and ChEC; genomic mapping of chromatin proteins. *Molecular Cell* **16**:147–157. DOI: <https://doi.org/10.1016/j.molcel.2004.09.007>, PMID: 15469830
- Schubert C**. 2018. Technology feature | ChIP off the old block: beyond chromatin immunoprecipitation. *Science* **362**:1193.2–111193. DOI: <https://doi.org/10.1126/science.362.6419.1193-b>
- Skene PJ**, Henikoff JG, Henikoff S. 2018. Targeted in situ genome-wide profiling with high efficiency for low cell numbers. *Nature Protocols* **13**:1006–1019. DOI: <https://doi.org/10.1038/nprot.2018.015>, PMID: 29651053
- Skene PJ**, Henikoff S. 2015. A simple method for generating high-resolution maps of genome-wide protein binding. *eLife* **4**:e09225. DOI: <https://doi.org/10.7554/eLife.09225>, PMID: 26079792
- Skene PJ**, Henikoff S. 2017. An efficient targeted nuclease strategy for high-resolution mapping of DNA binding sites. *eLife* **6**:e21856. DOI: <https://doi.org/10.7554/eLife.21856>, PMID: 28079019
- Teves SS**, An L, Hansen AS, Xie L, Darzacq X, Tjian R. 2016. A dynamic mode of mitotic bookmarking by transcription factors. *eLife* **5**:e22280. DOI: <https://doi.org/10.7554/eLife.22280>, PMID: 27855781
- Teytelman L**, Thurtle DM, Rine J, van Oudenaarden A. 2013. Highly expressed loci are vulnerable to misleading ChIP localization of multiple unrelated proteins. *PNAS* **110**:18602–18607. DOI: <https://doi.org/10.1073/pnas.1316064110>, PMID: 24173036
- Thakur J**, Henikoff S. 2018. Unexpected conformational variations of the human centromeric chromatin complex. *Genes & Development* **32**:20–25. DOI: <https://doi.org/10.1101/gad.307736.117>, PMID: 29386331
- Uyehara CM**, McKay DJ. 2019. A direct and widespread role for the nuclear receptor EcR in mediating the response to ecdysone in Drosophila. *bioRxiv*. DOI: <https://doi.org/10.1101/517458>
- van Galen P**, Viny AD, Ram O, Ryan RJ, Cotton MJ, Donohue L, Sievers C, Drier Y, Liao BB, Gillespie SM, Carroll KM, Cross MB, Levine RL, Bernstein BE. 2016. A multiplexed system for quantitative comparisons of chromatin landscapes. *Molecular Cell* **61**:170–180. DOI: <https://doi.org/10.1016/j.molcel.2015.11.003>, PMID: 26687680
- Weber CM**, Ramachandran S, Henikoff S. 2014. Nucleosomes are context-specific, H2A.Z-modulated barriers to RNA polymerase. *Molecular Cell* **53**:819–830. DOI: <https://doi.org/10.1016/j.molcel.2014.02.014>, PMID: 24606920
- Zhang W**, Chen Z, Yin Q, Zhang D, Racowsky C, Zhang Y. 2019. Maternal-biased H3K27me3 correlates with paternal-specific gene expression in the human morula. *Genes & Development* **33**:382–387. DOI: <https://doi.org/10.1101/gad.323105.118>, PMID: 30808660
- Zheng XY**, Gehring M. 2019. Low-input chromatin profiling in arabidopsis endosperm using CUT&RUN. *Plant Reproduction* **32**:63–75. DOI: <https://doi.org/10.1007/s00497-018-00358-1>, PMID: 30719569

